PEBBLE BED: REFLECTOR TREATMENT AND PRESSURE VELOCITY COUPLING

J.P.F. Charpin*, N.S. Kobo† K. Legodi‡, O.D. Makinde§
J.-M. T. Ngnotchouye¶, H. Ockendon‖, A.Z. Owinoh**
S. Peppin†† and J. Whiteley‡‡

Abstract

In this report we describe some models and numerical methods used to simulate the flow and temperature in a pebble bed modular reactor. The reactor core is filled with spherical particles containing low-enriched uranium. Helium gas is forced through the pebbles to absorb the tremendous amounts of generated heat. When modelling the reactor, numerical difficulties are encountered owing to large discontinuities in heat and mass fluxes at boundaries of the system. We first investigate the gas flow in the pebble region and find in the literature a resolution

*Department of Mathematics and Statistics, University of Limerick, Ireland, *email: jean.charpin@ul.ie*

†Department of Mechanical Engineering, Cape Peninsula University of Technology, Cape Town,

‡Department of Mathematics, Cape Peninsula University of Technology, Cape town

§Faculty of Engineering, Cape Peninsula University of Technology, Cape Town, *email: makinde@cput.ac.za*

¶Department of Mathematical Sciences, University of KwaZulu Natal, Pietermaritzburg, *email: ngnotchouye@ukzn.ac.za*

‖Oxford Centre for Industrial and Applied Mathematics, University of Oxford, United Kingdom,*email: ockendon@maths.ox.ac.uk*

**Department of Mathematics and Informatics, Free University of Berlin, Germany, *email: owinoch@minfu-berlin.de*

††Oxford Centre for Collaborative Applied Mathematics, University of Oxford, United Kingdom, *email: peppin@maths.ox.ac.uk*

‡‡Oxford Centre for Collaborative Applied Mathematics, University of Oxford, United Kingdom, *email: whiteley@maths.ox.ac.uk*

to the numerical issues. We then study the heat flow in the pebble region. Numerical schemes are presented that can significantly improve the accuracy of the computed results.

1 Introduction and problem description

A pebble bed modular reactor (PBMR) is a gas cooled nuclear reactor of approximately cylindrical shape. The reactor core is filled with fuel pebbles containing low-enriched uranium, located in an annular region close to the graphite centre of the reactor (Figure 1). During the reaction, helium flows through the hot pebbles to cool down the system. The heat from the nuclear reaction is transferred to the gas and converted into electricity through a turbine. PBMR Ltd aims to perform real-time accurate simulations of the helium flow and temperature in the pebbles. This is currently achieved by calculating the values of the required parameters for a very limited number of points. They asked the study group to investigate numerical difficulties they have encountered with the method they currently use. PBMR Ltd are looking for solutions that would allow them to keep their present finite volume numerical model on an unstructured grid.

Two types of numerical difficulties were encountered involving nonphysical variations in predicted velocities and temperatures at boundaries in the system. The first problem involves calculation of the flow of the hot gas. An abrupt change in the flow resistance is encountered when the gas enters the pebble bed. This causes unrealistic oscillations in the numerical solution around the gas-pebble interface. The second problem is related to simulations of heat flow between the pebble bed and reactor walls. Depending on the discretization used, large variations (up to 30 °C) in the temperature at the boundary are obtained. Refining the mesh removes the difference; however PBMR need to use a coarse mesh to enable real-time simulations. Both numerical difficulties have been resolved by a combination of related methods in the literature, and the development of new numerical methods based on integration and local analytical solutions. Details are given below, along with some thoughts on the appropriate physical modelling of the reactor core.

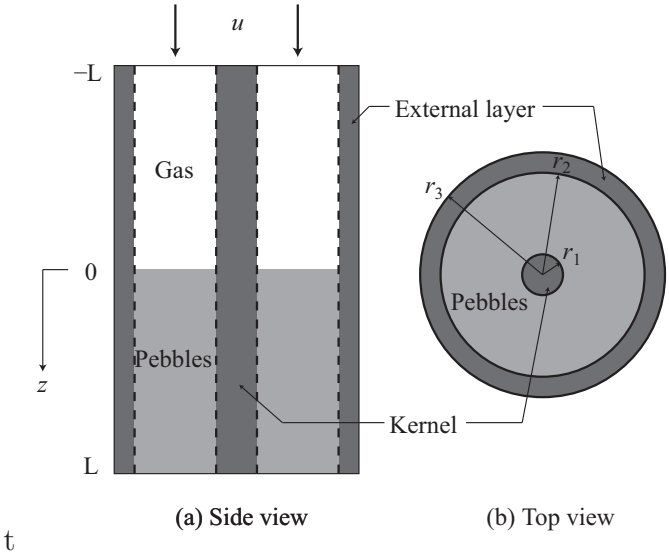

Figure 1: Schematic pebble bed nuclear reactor.

2 The governing equations

The reactor core is modelled as a cylindrical container as shown in Figure 1. The gas enters with velocity $\mathbf{u}$ at $z = -L$, flows over the hot pebbles which occupy the region $0 < z < L$ and leaves at $z = L$. Any general model of the reactor will involve coupled partial differential equations describing conservation of mass, momentum and energy in the system. However, the numerical difficulties experienced by PBMR Ltd can be illustrated by considering much simpler decoupled equations. We assume the gas is incompressible, with an average density ρ_g. The pebbles are stationary and we model them as a porous medium of constant porosity ϵ; they also act as a heat source q per unit volume. The pressures p_0 at $z = -L$ and p_1 at $z = L$ are prescribed. The flow of gas through the reactor is modelled by the incompressible Navier-Stokes equations:

$$\rho_g \left(\frac{\partial \mathbf{u}}{\partial t} + (\mathbf{u} \cdot \nabla)\mathbf{u} \right) = -\nabla p + \mu \nabla^2 \mathbf{u} - \mathbf{S}, \qquad \nabla \cdot \mathbf{u} = 0, \tag{1}$$

where $\mathbf{u}$ is the average fluid velocity on a scale much larger than a pebble diameter, $\mathbf{S}$ is a momentum sink term, and all the other variables are defined in the Nomenclature, Section 7. According to PBMR Ltd the gas flow in the

reactor is turbulent high Reynolds number flow. Therefore the momentum sink term S can be modelled as $\rho_g \lambda u^2$ in the pebbles (Ergun equation [1, 2]) and zero in $-L < z < 0$, where λ is a viscous resistance factor. The momentum sink term S plays the role of a large discontinuous body force and is known to lead to numerical difficulties [3]. We discuss these briefly in the next section and find a solution that allows PBMR Ltd to address the difficulties while continuing to use their basic finite volume code.

We are also concerned with the heat generated in the reactor and need to consider the mean temperature T_g in the gas and the mean temperature T_p in the pebbles. The energy equations for the gas and the pebbles can be written as

$$\rho_g c_g \left(\frac{\partial T_g}{\partial t} + \mathbf{u}_g \cdot \nabla T_g \right) = \nabla \cdot (\kappa_g \nabla T_g) + H(T_p - T_g), \tag{2}$$

$$\rho_p c_p \left(\frac{\partial T_p}{\partial t} \right) = \nabla \cdot (\kappa_p \nabla T_p) - H(T_p - T_g) + q, \tag{3}$$

where $\mathbf{u}_g = \mathbf{u}/\epsilon$, ϵ is the void fraction, H is a heat transfer coefficient, q is the heat generation, and these equations hold in $0 < z < L$, $r_1 < r < r_2$. We also need to consider the heat equation in the solid core, $0 < r < r_1$, and the external casing, $r_2 < r < r_3$, and then impose boundary conditions of continuous temperature and heat flux at the interfaces $r = r_1$, $r = r_2$.

We consider two simplified problems to test the numerical scheme. First we neglect the heat transfer to the gas and solve the steady-state version of equation (3) with $H = 0$. This problem is independent of z and it is solved analytically in Section 4.1. A further extension including the heat transfer term but assuming that T_g is constant can also be solved analytically as is shown in Section 4.2. Secondly we considered a one-dimensional model where T_g and T_p depend on z alone and (2) is solved in $-L < z < 0$ and (3) in $0 < z < L$. Since the numerical problems seem to be triggered by the discontinuity at $z = 0$ caused by the q term, we neglect the heat transfer term. Neither of these problems are physically realistic, but they have the advantage that they allow us to test out the numerics and show how the problems encountered by PBMR Ltd may be avoided.

3 Pressure velocity coupling

In this section we investigate the numerical solution of the equations governing the transport of cooling gas through the nuclear reactor. We first discuss

issues with standard numerical schemes that have been used to solve these equations (Section 3.1). We then discuss, in Section 3.2 the application of a novel scheme to circumvent the difficulties. We conclude by briefly discussing other techniques that may be used to solve the governing equations.

3.1 Standard numerical techniques

A common technique used for computing the numerical solution of the Navier–Stokes equations is the *finite volume technique*: see, for example, Tannehill *et al.* [4]. This method underpins the SIMPLE algorithm [5] which may be summarised as follows.

1. Guess the pressure field p_0.
2. Solve the momentum equation (1a) to calculate $\mathbf{u}$.
3. Use the continuity equation (1b) to update the pressure p.
4. Update the velocity field using $\mathbf{u}_{new} = \mathbf{u}_{old} - A\nabla p$.
5. Repeat steps 2–5 until the solution has converged.

The constant A is a fictitious time increment divided by the density. As far as implementation of the algorithm goes, it is a relaxation constant, and needs to be sufficiently high to allow the iterate for $\mathbf{u}$ to vary on each iteration, but sufficiently small for convergence [4].

PBMR have software that implements the SIMPLE algorithm. This software has much more functionality than the fluid dynamics discussed here: as such PBMR are reluctant to implement significant changes to the fluid dynamics component of this software as it may impact elsewhere in the software. As a consequence, the SIMPLE algorithm must be implemented using a cell–centred finite volume method.

The drawback to implementing the SIMPLE algorithm using a cell–centred finite volume mesh is that the phenomenon known as *pressure–velocity uncoupling* occurs. This can sometimes be avoided by the use of Rhie–Chow interpolation [6]. However, this technique does not work well when there are rapid changes in body force, such as those appearing in our model problem in Section 2. When applied to the model problem, this technique induces 'spikes' in the computed velocity rather than a constant velocity. This is demonstrated in Figure 2, where the computed velocity is shown by the solid line and the pressure shown by a broken line.

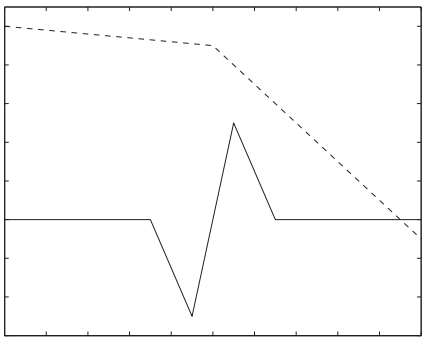

Figure 2: Velocity spikes: the solution of the model problem described in Section 2 using the SIMPLE algorithm with Rhie-Chow interpolation. The solid line represents the velocity, and the broken line represents the pressure.

3.2 A more appropriate numerical technique

The issue of velocity spikes was addressed by Mencinger and Žun [3] who modelled abrupt changes in the force field due to two mixed fluids, e.g. air bubbles in water. The key to this algorithm is the discretisation of the momentum sink: these terms should be discretised on the faces of the control volumes rather than at the cell centres. When this is done, the velocity spikes shown in Figure 2 are removed, and the velocity is given by a constant function as required.

This method appears to solve the problem encountered by PBMR, although there are some words of warning. As the momentum sink is dependent on $\mathbf{u}$, this quantity must first be calculated from the values at the cell–centres. Although this is not exactly what is desired by PBMR, it is likely to be a small modification to the code that is unlikely to cause any difficulties.

3.3 Discussion on pressure–velocity coupling

It should be noted that the SIMPLE algorithm was developed in 1980, and that the Rhie–Chow interpolation scheme was developed in 1983. The need to develop uncoupled algorithms such as these was largely dictated by computational resources—particularly memory—available at that time. However, the significant and steady increase in computer power that has been witnessed

during the past 30 years has spawned the development of many more robust finite–volume methods (FVMs) and finite–element methods (FEMs): although implementation of these methods would not have been possible on earlier machines, they are now often the method of choice. Of particular interest are FEMs. These methods are based on a more sophisticated mathematical basis, and therefore allow desirable features such as stability to be implemented in a mathematically rigorous fashion. Furthermore, the abstract mathematical formulation on which these methods are based lends itself to rigorous error analysis techniques, from which automatic mesh refinement routines may be derived to ensure the error is within a given tolerance. These techniques do, however, require the (computationally memory intensive) solution of large systems of equations, and so have only recently become popular for large scale computations. For more details on the application of FEMs to the solution of the Navier–Stokes equation see Elman *et al.* [7] and the references therein. Should PBMR ever decide to significantly overhaul their software they may wish to use these more robust algorithms.

4 Reflector treatment

The temperature in the pebble bed will now be studied. Two cases will be considered to solve the steady state numerical difficulties encountered by PBMR Ltd:

- A simplified (non-physically realistic) solution where no heat may be transferred to the gas. This case admits straightforward analytical solutions that considerably simplifies comparisons between analytical and numerical solutions.
- A more general system will then be considered. Analytical solutions involving Bessel functions are also available and the method developed for the simplified case will be extended.

When expansions are necessary for numerical solutions, they only include the terms necessary to achieve accurate approximations.

4.1 Simplified case

The configuration studied in this section is presented in Figure 3. Heat is only released in Region 2 at the constant rate q. In this case, the governing

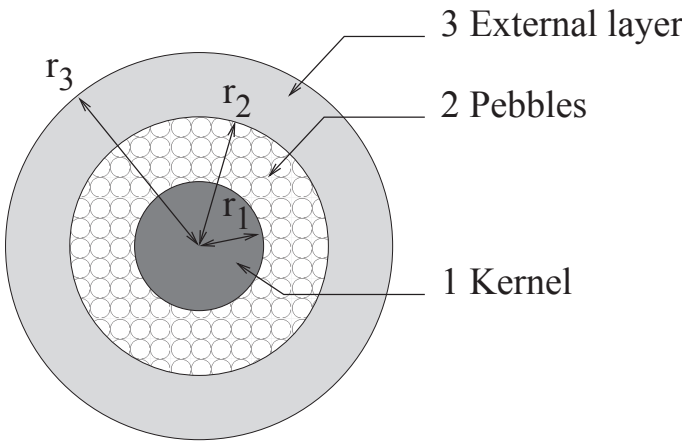

Figure 3: Simplified case configuration.

equations may be written:

$$0 \leq r \leq r_1 : \qquad -\frac{1}{r}\frac{\partial}{\partial r}\left(\kappa_1 r \frac{\partial T}{\partial r}\right) = 0 \ , \tag{4}$$

$$r_1 \leq r \leq r_2 : \qquad -\frac{1}{r}\frac{\partial}{\partial r}\left(\kappa_2 r \frac{\partial T}{\partial r}\right) = q \ , \tag{5}$$

$$r_2 \leq r \leq r_3 : \qquad -\frac{1}{r}\frac{\partial}{\partial r}\left(\kappa_3 r \frac{\partial T}{\partial r}\right) = 0 \ , \tag{6}$$

subject to the boundary conditions

$$T\left(r_3\right) = T_{ref} \ , \ \left.\frac{\partial T}{\partial r}\right|_{r=0} = 0 \ . \tag{7}$$

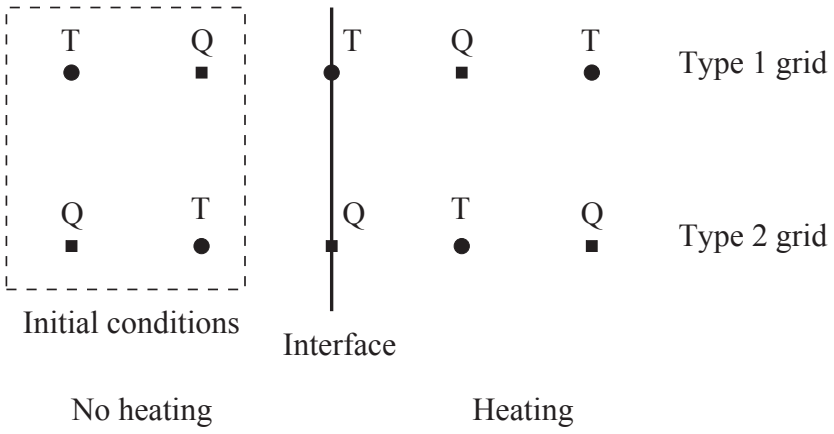

Figure 4: Typical grids.

Using the continuity of temperatures and heat fluxes, the following analytical solution may be calculated:

$$0 \le r \le r_1 : \qquad T = T_0 - \frac{q}{2\kappa_3}\left(r_2^2 - r_1^2\right)\ln\left(\frac{r_2}{r_3}\right) - \frac{q}{4\kappa_2}\left(r_1^2 - r_2^2\right) + \frac{qr_1^2}{2\kappa_2}\ln\left(\frac{r_1}{r_2}\right), \quad (8)$$

$$r_1 \le r \le r_2 : \qquad T = T_0 - \frac{q}{2\kappa_3}\left(r_2^2 - r_1^2\right)\ln\left(\frac{r_2}{r_3}\right) - \frac{q}{4\kappa_2}\left(r^2 - r_2^2\right) + \frac{qr_1^2}{2\kappa_2}\ln\left(\frac{r}{r_2}\right), \quad (9)$$

$$r_2 \le r \le r_3 : \qquad T = T_0 - \frac{q}{2\kappa_3}\left(r_2^2 - r_1^2\right)\ln\left(\frac{r}{r_3}\right). \quad (10)$$

Numerical schemes are derived for the system (4-6) on the two types of grids described on Figure 4. In each case, the space step is Δx. The position of the points will vary:

- Type 1 grids. The temperatures are calculated at positions $x = i\Delta x$ and the fluxes are evaluated at $x = (i + 1/2)\Delta x$. The temperature T_i and the flux $Q_{i+1/2}$ should be expressed as functions of the initial conditions T_{i-1} and $Q_{i-1/2}$, where $Q = -\kappa\partial T/\partial r$ is the standard one-dimensional heat flux in cylindrical polar coordinates.

- Type 2 grids. The temperatures are calculated at positions $x = (i + 1/2)\Delta x$ and the fluxes are evaluated at $x = i\Delta x$. The temperature $T_{i+1/2}$ and the flux Q_i should be expressed as functions of the initial conditions $T_{i-1/2}$ and Q_{i-1}.

The objective here is to get the same quality of results on both grid types. The temperature will be calculated from the centre, $r = 0,\ i = 0$ towards the external boundary, $r = r_3,\ i = i_3$. Boundary conditions are at the two different extremities of the domain. In this simplified set-up, replacing the temperature, T, with $T + T_m$, where T_m is a constant temperature, will not affect the result because the heat source q is constant. The temperature $T = 0$ may be imposed at the centre, and once the temperature profile has been determined, the value of T_m is then chosen so the boundary condition $T(r_3) = T_{ref}$ is satisfied. The numerical scheme will be detailed for each of the three zones. Exact and approximate expressions are given for fluxes and temperatures in all possible cases.

4.1.1 Zone 1&3: Kernel and external layer

Integrating equation (4) or (6) between α and r leads to:

$$\int_r^\alpha \frac{\partial}{\partial r}\left[\kappa r \frac{\partial T}{\partial r}\right] dr = 0 \Longleftrightarrow \quad Q = \frac{r_\alpha}{r} Q_\alpha \ .$$

Integrating the equation once more between a and r provides the relation:

$$T = T_a - \frac{r_\alpha Q_\alpha}{\kappa} \ln\left(\frac{r}{a}\right) \ .$$

Using appropriate values for the dummy variables α and a leads to the following numerical schemes:

- Type 1 grid

$$\begin{aligned} Q_{i+1/2} &= \frac{r_{i-1/2}}{r_{i+1/2}} Q_{i-1/2} = Q_{i-1/2}\left(1 - \frac{\Delta r}{r_{i+1/2}}\right) \ , \\ T_{i+1} &= T_i - \frac{r_{i+1/2} Q_{i+1/2}}{\kappa} \ln\left(\frac{r_{i+1}}{r_i}\right) = T_i - \frac{Q_{i+1/2}\Delta r}{\kappa} \ . \end{aligned}$$

- Type 2 grid

$$\begin{aligned} Q_i &= \frac{r_{i-1}}{r_i} Q_{i-1} = Q_{i-1}\left(1 - \frac{\Delta r}{r_i}\right) , \\ T_{i+1/2} &= T_{i-1/2} - \frac{r_i Q_i}{\kappa} \ln\left(\frac{r_{i+1/2}}{r_{i-1/2}}\right) = T_{i-1/2} - \frac{Q_i \Delta r}{\kappa} . \end{aligned}$$

4.1.2 Zone 2: Temperature in the pebbles

Similar integrations of equation (5) lead to the following equations:

- Type 1 grid

$$\begin{aligned} Q_{i+1/2} &= \frac{r_{i-1/2}}{r_{i+1/2}} Q_{i-1/2} + q\frac{r_{i+1/2}^2 - r_{i-1/2}^2}{2r_{i+1/2}} \\ &= Q_{i-1/2}\left(1 - \frac{\Delta r}{r_{i+1/2}}\right) + q\Delta r - \frac{q\Delta r^2}{2r_{i+1/2}} , \\ T_{i+1} &= T_i + \left(\frac{q r_{i+1/2}^2}{2\kappa_2} - \frac{r_{i+1/2} Q_{i+1/2}}{\kappa_2}\right) \ln\left(\frac{r_{i+1}}{r_i}\right) - \frac{q}{4\kappa_2}\left(r_{i+1}^2 - r_i^2\right) \\ &= T_i - \frac{Q_{i+1/2}\Delta r}{\kappa_2} . \end{aligned}$$

- Type 2 grid

$$\begin{aligned} Q_i &= \frac{r_{i-1}}{r_i} Q_{i-1} + q\frac{r_i^2 - r_{i-1}^2}{2r_i} = Q_{i-1}\left(1 - \frac{\Delta r}{r_i}\right) + q\Delta r - \frac{q\Delta r^2}{2r_i} , \\ T_{i+1/2} &= T_{i-1/2} + \left(\frac{q r_i^2}{2\kappa_2} - \frac{r_i Q_i}{\kappa_2}\right) \ln\left(\frac{r_{i+1/2}}{r_{i-1/2}}\right) - \frac{q}{4\kappa_2}\left(r_{i+1/2}^2 - r_{i-1/2}^2\right) \\ &= T_{i-1/2} - \frac{Q_i \Delta r}{\kappa_2} . \end{aligned}$$

4.1.3 Interface zone 1-zone 2

The position of the interface is $r_1 = i_1 \Delta r$.

- Type 1 grid

$$\begin{aligned} Q_{i_1+1/2} &= \frac{r_{i_1-1/2}}{r_{i_1+1/2}} Q_{i_1-1/2} + \frac{q}{2} \frac{r_{i_1+1/2}^2 - r_{i_1}^2}{r_{i_1+1/2}} \\ &= Q_{i_1-1/2} \left(1 - \frac{\Delta r}{r_{i_1+1/2}}\right) + \frac{q}{2} \Delta r - \frac{q \Delta r^2}{8 r_{i_1+1/2}} \ , \\ T_{i_1+1} &= T_{i_1} + \frac{q r_{i_1+1/2}^2/2 - r_{i_1+1/2} Q_{i_1+1/2}}{\kappa_2} \ln\left(\frac{r_{i_1+1}}{r_{i_1}}\right) - \frac{q}{4\kappa_2} \left(r_{i_1+1}^2 - r_{i_1}^2\right) \\ &= T_{i_1} - \frac{Q_{i_1+1/2} \Delta r}{\kappa_2} \ . \end{aligned}$$

- Type 2 grid

$$\begin{aligned} Q_{i_1} &= \frac{r_{i_1-1}}{r_{i_1}} Q_{i_1-1} = Q_{i_1-1} \left(1 - \frac{\Delta r}{r_{i_1}}\right) \ , \\ T_{i_1+1/2} &= T_{i_1-1/2} + \left(\frac{q r_{i_1}^2}{2\kappa_2} - \frac{r_{i_1} Q_{i_1}}{\kappa_2}\right) \ln\left(\frac{r_{i_1+1/2}}{r_{i_1}}\right) - \frac{q}{4\kappa_2} \left(r_{i_1+1/2}^2 - r_{i_1}^2\right) \\ &= T_{i_1-1/2} - \frac{Q_{i_1} \Delta r}{2\kappa_2} + \left(\frac{Q_{i_1}}{8 r_{i_1} \kappa_2} - \frac{q}{8\kappa_2}\right) \Delta r^2 \ . \end{aligned}$$

4.1.4 Interface zone 2-zone 3

The position of the interface is $r_2 = i_2 \Delta r$.

- Type 1 grid

$$\begin{aligned} Q_{i_2+1/2} &= \frac{r_{i_2-1/2}}{r_{i_2+1/2}} Q_{i_2-1/2} + \frac{q}{2} \frac{r_{i_2}^2 - r_{i_2-1/2}^2}{r_{i_2+1/2}} \\ &= Q_{i_2-1/2} \left(1 - \frac{\Delta r}{r_{i_2+1/2}}\right) + \frac{q}{2} \Delta r - \frac{3 q \Delta r^2}{8 r_{i_2+1/2}} T_{i_2+1} \\ &= T_{i_2} - \frac{r_{i_2+1/2} Q_{i_2+1/2}}{\kappa_3} \ln\left(\frac{r_{i_2+1}}{r_{i_2}}\right) \\ &= T_{i_2} - \frac{Q_{i_2+1/2} \Delta r}{\kappa_3} \ . \end{aligned}$$

- Type 2 grid

$$\begin{aligned} Q_{i_2} &= \frac{r_{i_2-1}}{r_{i_2}} Q_{i_2-1} + q\frac{r_{i_2}^2 - r_{i_2-1}^2}{2r_{i_2}} = Q_{i_2-1}\left(1 - \frac{\Delta r}{r_{i_2}}\right) \\ &\quad + q\Delta r - \frac{q\Delta r^2}{2r_{i_2}} T_{i_2+1/2} \\ &= T_{i_2-1/2} - r_{i_2} Q_{i_2}\left[\frac{1}{\kappa_2}\ln\left(\frac{r_{i_2}}{r_{i_2-1/2}}\right) + \frac{1}{\kappa_3}\ln\left(\frac{r_{i_2+1/2}}{r_{i_2}}\right)\right] \\ &\quad + \frac{q r_{i_2}^2}{2\kappa_2}\ln\left(\frac{r_{i_2}}{r_{i_2-1/2}}\right) - \frac{q}{4\kappa_2}\left(r_{i_1}^2 - r_{i_1-1/2}^2\right) \\ &= T_{i_2-1/2} - Q_{i_2}\Delta r\left(\frac{1}{2\kappa_2} + \frac{1}{2\kappa_3}\right) + \left(\frac{Q_{i_2}}{8r_{i_2}}\left(\frac{1}{\kappa_3} - \frac{1}{\kappa_2}\right)\right. \\ &\quad \left. + \frac{q}{8\kappa_2}\right)\Delta r^2 \,. \end{aligned}$$

4.1.5 Numerical results

Figure 5 compares the numerical results calculated with expansions and the analytical solution for the space step $\Delta r = 0.5$, which means two points per zone. This is the coarsest possible mesh, on this grid the error should be maximum. The results are evaluated using first order in Δr approximations for the temperature and second order approximations in Δr for the fluxes. The second order approximation significantly increases accuracy and compensates the effects of the coarse grid. A second order approximation in Δr is also necessary at the interfaces for the type 2 grid, otherwise, the heat produced in the pebbles would not influence the temperature on the cell. In this situation, the temperature calculated with either grid is very close to the analytical solution: the maximum difference observed, ΔT, occurs in the flat central region and $\Delta T \leq 2^o C$ for both curves. This difference satisfies $\Delta T \leq 0.5^o C$ if the number of points is doubled. Without second order expansions in Δr, for $\Delta r = 0.5$ the difference between analytical and numerical results reaches $\Delta T = 60^o C$ for the type 1 grid and $\Delta T = 100^o C$ for the type 2 grid. Using a second order approximation in Δr for the fluxes and the interfaces of the type 2 grid is absolutely necessary to improve the accuracy of the numerical results. For comparison, first order results are included in Figure 5.

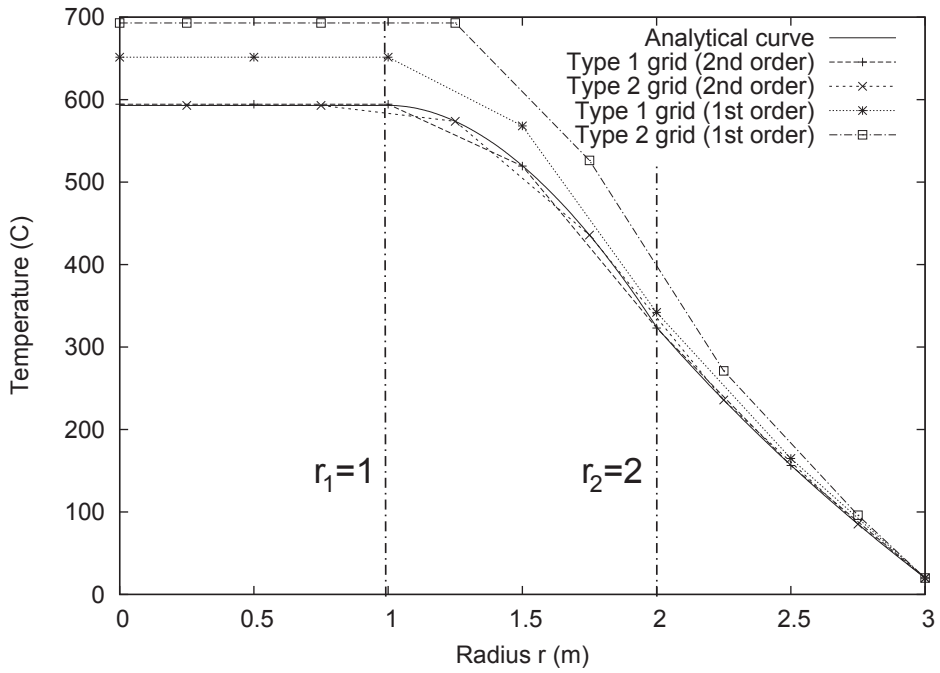

Figure 5: Comparison of the various schemes for the simplified model. Note the radius is measured along the horizontal axis.

4.2 More general system

A more general configuration will now be studied. In this case, the governing equations may be written:

$$0 \leq r \leq r_1 : \qquad -\frac{1}{r}\frac{\partial}{\partial r}\left(\kappa_1 r \frac{\partial T}{\partial r}\right) = 0 \ , \tag{11}$$

$$r_1 \leq r \leq r_2 : \qquad -\frac{1}{r}\frac{\partial}{\partial r}\left(\kappa_2 r \frac{\partial T}{\partial r}\right) = q + H\left(T_g - T\right) \ , \tag{12}$$

$$r_2 \leq r \leq r_3 : \qquad -\frac{1}{r}\frac{\partial}{\partial r}\left(\kappa_3 r \frac{\partial T}{\partial r}\right) = 0 \ , \tag{13}$$

subject to the boundary conditions

$$T\left(r_3\right) = T_{ref} \ , \ \left.\frac{\partial T}{\partial r}\right|_{r=0} = 0 \ . \tag{14}$$

An analytical solution may be calculated for the system (11-14). This is detailed in Appendix B. The numerical scheme will be calculated for both type 1 and type 2 grids using the same methods as in the previous section.

4.2.1 Zone 2: temperature in the pebbles

- Type 1 grid

$$\begin{aligned} Q_{i+1/2} &= -H\left(T_{i-1/2}-\frac{q-HT_g}{H}\right)\left(\Delta r-\frac{\Delta r^2}{2r_i}+\frac{\Delta r^3}{4r_i^2}+\frac{H\Delta r^3}{24\kappa_2}\right) \\ &\quad +Q_{i-1/2}\left(1-\frac{\Delta r}{r}+\frac{\Delta r^2}{2r_i^2}+\frac{H\Delta r^3}{24\kappa_2 r_i}-\frac{\Delta r^3}{4r_i^3}\right), \\ T_{i+1} &= T_i-\frac{Q_{i+1/2}\Delta r}{\kappa_2}. \end{aligned}$$

- Type 2 grid

$$\begin{aligned} Q_i &= Q_{i-1}\left(1-\frac{\Delta r}{r_i}+\frac{H\Delta r^3}{24\kappa_2 r_i}\right) \\ &\quad -H\left(T_{i_1-1/2}-\frac{q-HT_g}{H}\right)\left(\Delta r-\frac{\Delta r^2}{2r_i}-\frac{H\Delta r^3}{24\kappa_2}\right), \\ T_{i+1/2} &= T_{i-1/2}-\frac{Q_i\Delta r}{\kappa_2}. \end{aligned}$$

4.2.2 Interface zone 1-zone 2

- Type 1 grid

$$\begin{aligned} Q_{i_1+1/2} &= -H\left(T_{i_1-1/2}-\frac{q-HT_g}{H}\right)\left(\frac{\Delta r}{2}-\frac{\Delta r^2}{8r_{i_1}}+\frac{H\Delta r^3}{48\kappa_2}+\frac{\Delta r^3}{16r_{i_1}^2}\right) \\ &\quad +Q_{i_1-1/2}\left(1-\frac{\Delta r}{2r_{i_1}}+\frac{H\Delta r^2}{8\kappa_2}+\frac{\Delta r^2}{4r_{i_1}^2}-\frac{H\Delta r^3}{24\kappa_2 r_{i_1}}-\frac{\Delta r^3}{24r_{i_1}^3}\right), \\ T_{i_1+1} &= T_{i_1}-\frac{Q_{i_1+1/2}\Delta r}{\kappa_2}. \end{aligned}$$

- Type 2 grid

$$\begin{aligned} Q_{i_1} &= \frac{r_{i_1-1}}{r_{i_1}} Q_{i_1-1} = Q_{i_1-1}\left(1-\frac{\Delta r}{r_{i_1}}\right), \\ T_{i_1+1/2} &= T_{i_1-1/2} + \left(\frac{HT_{i_1-1/2}}{\kappa_2} - \frac{q+HT_g}{\kappa_2}\right)\left(\frac{\Delta r^2}{8} - \frac{\Delta r^3}{48 r_{i_1}}\right) \\ &\quad + \frac{Q_{i_1}}{\kappa_2}\left(\frac{\Delta r}{2} - \frac{3\Delta r^2}{8 r_{i_1}} - \frac{H\Delta r^3}{24\kappa_2} + \frac{9\Delta r^3}{48 r_{i_1}^2}\right). \end{aligned}$$

4.2.3 Interface zone 2-zone 3

- Type 1 grid

$$\begin{aligned} Q_{i_2+1/2} &= -H\left(T_{i_2-1/2} - \frac{q-HT_g}{H}\right)\left(\frac{\Delta r}{2} - \frac{3\Delta r^2}{8 r_{i_2}} - \frac{H\Delta r^3}{24\kappa_2} + \frac{3\Delta r^3}{16 r_{i_2}^2}\right) \\ &\quad + Q_{i_2-1/2}\left(1 - \frac{\Delta r}{r_{i_2}} + \frac{\Delta r^2}{r_2^2} - \frac{H\Delta r^2}{8\kappa_2} + \frac{7H\Delta r^3}{48\kappa_2 r_{i_2}} - \frac{\Delta r^3}{4 r_{i_2}^3}\right), \\ T_{i_2+1} &= T_{i_2} - \frac{Q_{i_2+1/2}\Delta r}{\kappa_3}. \end{aligned}$$

- Type 2 grid

$$\begin{aligned} Q_{i_2} &= Q_{i_2-1}\left(1 - \frac{\Delta r}{r_{i_2}} + \frac{H\Delta r^3}{24\kappa_2 r_{i_2}}\right) \\ &\quad - H\left(T_{i_2-1/2} - \frac{q-HT_g}{H}\right)\left(\Delta r - \frac{\Delta r^2}{2 r_{i_2}} - \frac{H\Delta r^3}{24\kappa_2}\right), \\ T_{i_2+1/2} &= T_{i_2-1/2} - \frac{H}{\kappa_2}\left(T_{i_2-1/2} - \frac{q-HT_g}{H}\right)\left(\frac{3\Delta r^2}{8} - \frac{7\Delta r^3}{48 r_{i_2}}\right) \\ &\quad + \frac{Q_{i_2-1}}{\kappa_2}\left(-\frac{\Delta r}{2} + \frac{3\Delta r^2}{8 r_{i_2}} + \frac{\Delta r^3}{12 r_{i_2}^2} + \frac{H\Delta r^3}{24\kappa_2 r_{i_2}^2}\right) \\ &\quad + Q_{i_2}\left(\frac{\Delta r}{2\kappa_3} - \frac{\Delta r^2}{8\kappa_3 r_{i_2}} + \frac{\Delta r^3}{24\kappa_3 r_{i_2}^2}\right). \end{aligned}$$

4.2.4 Numerical results

Figure 6 compares the numerical results calculated with expansions and the analytical solution for the space step $\Delta r = 0.5$, which again means two points

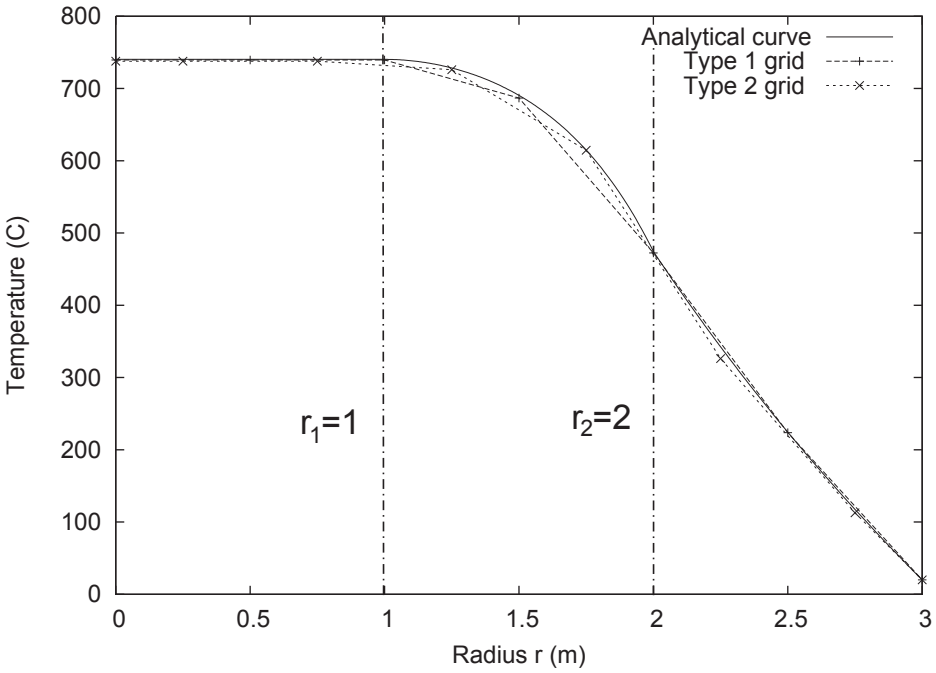

Figure 6: Comparison of the various schemes for the more general model. Note the radius is measured along the horizontal axis.

per zone. The temperatures calculated with either grid are again really close to the analytical results. The differences is less than $\Delta T = 4^oC$ for all points except for the type 2 grid after the second interface, where the error is $\Delta T = 16.5^oC$. Here again, the error is reduced when the space step gets lower: the maximum error is $\Delta T \leq 4.5^oC$ for $\Delta r = 0.25$ with all other points except for one are calculated with an error less than $\Delta T \leq 1.5^oC$. The error is mainly due to the approximation of the flux. If accuracy may not be achieved with the third order accuracy in Δr for large values of the space step, using the exact solution of the flux could be a better option. For grids of type 1 and type 2, first order approximations in Δr lead to errors up to 50^oC. The errors occur around $r = 2$. They would be difficult to see on Figure 6 so the first order curves are not included.

These results were calculated with gas temperature $T_g = 700^oC$. This temperature will vary significantly with the position in the vessel. This aspect will now be studied more carefully.

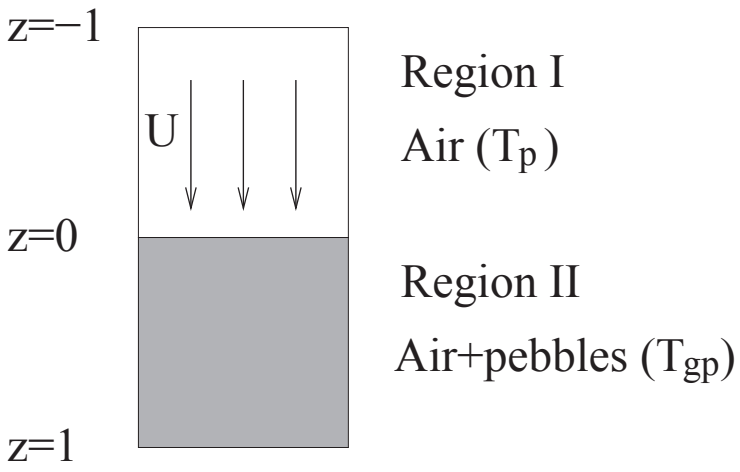

Figure 7: Simple geometry of the system.

5 Temperature variation of gas in the pebbles

The temperature of the gas flow through the pebble bed will now be considered. We model the pebble bed reactor as a uniform channel with two distinct Regions I & II, see Figure 7. In Region I, a cooling gas of temperature T_g flows with constant mean velocity U (averaged over the cross section of the channel) towards Region II which is occupied by pebbles. This region has a constant void fraction, ϵ, and heat source, q, and an adiabatic end. The temperature of the gas in Region II is denoted T_{gp}. The effect of heat transfer from the pebbles to the gas is modelled as an effective heat source q in the gas.

5.1 Model

For this one dimensional system, the steady state heat equations may be written:

$$-\rho_g c_g U \frac{\partial T_g}{\partial z} = \kappa_g \frac{\partial^2 T_g}{\partial z^2} \quad \text{in Region I} \quad -L \le z \le 0, \tag{15}$$

$$-\rho_g c_g \frac{U}{\epsilon} \frac{\partial T_{gp}}{\partial z} = \kappa_g \frac{\partial^2 T_{gp}}{\partial z^2} + q \quad \text{in Region II} \quad 0 \le z \le L, \tag{16}$$

and all the quantities are defined in the Nomenclature, Section 7. To simplify the problem, all quantities are assumed constant. Equations (15) and (16) are solved subject to the following boundary conditions:

- Imposed temperature at $z = -L$:

$$T_g(-L) = T_0 \ ,$$

- Adiabatic condition at $z = L$:

$$\left.\frac{\partial T_{gp}}{\partial z}\right|_{z=L} = 0 \ ,$$

- Continuity of temperature and fluxes at the interface

$$\begin{aligned} T_g(0) &= T_{gp}(0) \\ \left.\frac{\partial T_g}{\partial z}\right|_{z=0} &= \left.\frac{\partial T_{gp}}{\partial z}\right|_{z=0} \ . \end{aligned}$$

  The flux condition may be simplified since the conduction is the same on either side of the interface.

The length and temperature are non-dimensionalised as follows:

$$z = Lz' \ , \qquad T = T_0 + \Delta T T' \ ,$$

where L is the typical height, T_0 is the initial temperature of the gas and ΔT a typical temperature gap. The governing equations become

$$\begin{aligned} \frac{\partial T_g}{\partial z} &= -\frac{\kappa_g}{\rho_g c_g L U}\frac{\partial^2 T_g}{\partial z^2}, \\ \frac{\partial T_{gp}}{\partial z} &= -\frac{\epsilon\kappa_g}{\rho_g c_g L U}\frac{\partial^2 T_{gp}}{\partial z^2} - \frac{\epsilon L q}{\rho_g c_g \Delta T U} \ . \end{aligned}$$

Diffusion is a slow phenomenon, so clearly, the temperature is governed by convection and the heat source. The typical temperature gap is therefore:

$$\Delta T = \frac{\epsilon L q}{\rho_g c_g U} \ .$$

The governing equations are then

$$\frac{\partial T_g}{\partial z} = -\kappa_1 \frac{\partial^2 T_g}{\partial z^2} \ , \tag{17}$$

$$\frac{\partial T_{gp}}{\partial z} = -\epsilon\kappa_1 \frac{\partial^2 T_{gp}}{\partial z^2} - 1 \ , \tag{18}$$

subject to the boundary condition

$$
\begin{aligned}
T_g(-1) &= 0 \ , && (19)\\
\left.\frac{\partial T_{gp}}{\partial z}\right|_{z=1} &= 0 \ , && (20)\\
T_g(0) &= T_{gp}(0) \ , && (21)\\
\left.\frac{\partial T_g}{\partial z}\right|_{z=0} &= \left.\frac{\partial T_{gp}}{\partial z}\right|_{z=0} \ , && (22)
\end{aligned}
$$

where

$$\kappa_1 = \frac{\kappa_g}{\rho_g c_g L U} \ .$$

Equations (17–22) may be easily solved:

$$
\begin{aligned}
T_g &= A + B e^{-z/\kappa_1} \ , && (23)\\
T_{gp} &= C + D e^{-z/(\epsilon\kappa_1)} - z \ , && (24)
\end{aligned}
$$

where

$$
\begin{aligned}
A &= -\kappa_1 e^{1/\kappa_1}\left(1 - e^{1/(\epsilon\kappa_1)}\right) \ ,\\
B &= \kappa_1\left(1 - e^{1/(\epsilon\kappa_1)}\right) \ ,\\
C &= \epsilon\kappa_1 e^{1/(\epsilon\kappa_1)} + \kappa_1\left(1 - e^{1/(\epsilon\kappa_1)}\right)\left(1 - e^{1/\kappa_1}\right) \ ,\\
D &= -\epsilon\kappa_1 e^{1/(\epsilon\kappa_1)} \ .
\end{aligned}
$$

5.2 Numerical results

The temperature of the air is plotted in Figure 8 for $\kappa_1 = 0.1,\ 1,\ 10$. The results are dimensionalised to fit with experimental results: at the top of the pressure vessel, the temperature is $T = 500^oC$ and at the bottom $T = 900^oC$. These curves correspond to $\epsilon = 0.1$. The curves calculated with $\epsilon = 0.3$ are very close to the curves obtained in Figure 8. The parameter κ_1 seems to have more influence. The value of this parameter depends on the thermal properties of the gas and the velocity of the gas. These values were taken constant but should vary with the gas temperature and pressure. The results are therefore only a first approximation.

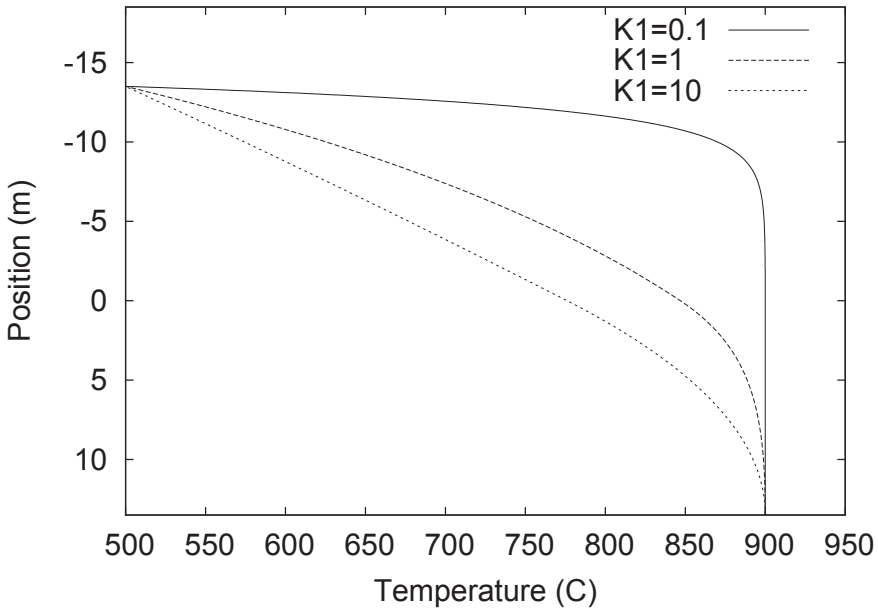

Figure 8: Gas temperature profiles for various values of κ_1. The top of the reactor corresponds to $z = -13.5m$ and the bottom $z = 13.5m$.

6 Conclusion and future work

The study group provided insights on the gas flow model inside the pebbles and suggested solutions for the numerical problems encountered by PBMR Ltd.

- The velocity spikes observed numerically at the surface of the pebbles may be removed by employing a more appropriate numerical method. The crux of the problem is the discretisation of the sink terms: they should be evaluated at the boundaries of the grid cells and not at the centre.

- The numerical problems due to the two different types of grids may be solved by using specially designed numerical schemes. To achieve maximum accuracy, the formulae should be based on local analytical solutions of the governing equations. The formulae can be approximated using Taylor series expansions as in Section 4. Depending on the position and

parameter, first, second or third order Taylor expansions are required to guarantee that the numerical solutions are close enough to the analytical solution. The method was developed for specific grid positions relative to interfaces. If necessary, the method could be extended to more general cases using a similar approach.

The temperature in the pebbles was calculated in each cross section of the pressure vessel. The evolution of the temperature in the axis direction was neglected, although this was shown to vary significantly. Vertical heat conduction should be investigated to further increase the accuracy of the numerical simulations.

Acknowledgements

All contributors would like to thank Mr Onno Ubbink from Pebble Bed Modular Reactor (Pty) Limited (PBMR) for introducing the problem and assisting in answering questions. This publication is based on work supported in part by Award No KUK-C1-013-04, made by King Abdullah University of Science and Technology (KAUST). J.P.F. Charpin acknowledges the support of the Mathematics Application Consortium for Science and Industry funded by the Science Foundation Ireland mathematics initiative Grant No 06/MI/005 (www.macsi.ul.ie).

7 Nomenclature

α	Heat transfer coefficient		$W{\cdot}m^{-2}{\cdot}K^{-1}$
ϵ	Void fraction	$0-1$	ND
κ	Thermal conductivity	$\kappa_1 = 10$, $\kappa_2 = 15$, $\kappa_3 = 20$	$W{\cdot}m^{-1}{\cdot}K^{-1}$
λ	Inertial resistance factor		m^{-1}
μ	Dynamic viscosity		$kg{\cdot}m^{-1}{\cdot}s^{-1}$
ρ	Density		$kg{\cdot}m^{-3}$
Δr, Δx, Δy	Space steps in the r, x and y directions		m
c	Heat capacity		$J{\cdot}kg^{-1}{\cdot}K^{-1}$
p	Pressure		Pa
q	Heat source	10000	$W{\cdot}m^{-3}$
$r,\ x,\ y$	Radial and Cartesian coordinates		m
t	Time		s
$\vec{v} = (u, v)$	Velocity in x and y directions		$m{\cdot}s^{-1}$
H	Non-standard heat transfer coefficient		$W{\cdot}m^{-3}{\cdot}K^{-1}$
Q	Heat flux		$W{\cdot}m^{-2}$
Re	Reynolds number		
$S = (S_x,\ S_y)$	Momentum sink term		$m{\cdot}s^{-2}$
T	Temperature		K
U	Cross-sectional average gas velocity		$m{\cdot}s^{-1}$

Subscripts

p, Pebbles, g, Gas gp, Gas in the pebbles.

References

[1] Bird, R.B., Stewart, W.E. and Lightfoot, E.N. Transport Phenomena. John Wiley & Sons, New York, USA, 1960.

[2] Fowler, A.C. Mathematical Models in the Applied Sciences. Cambridge University Press, Cambridge, UK, 1997.

[3] Mencinger, J. and Žun, I. On the finite volume discretization of discontinuous body force field on collocated grid: Application to VOF method. *Journal of Computational Physics*, **221**, (2007), 524–538.

[4] Tannehill, J.C., Anderson, D.A. and Pletcher, R.H. Computational Fluid Mechanics and Heat Transfer. Taylor & Francis, Philadelphia, PA, USA, 1997.

[5] Patankar, S.V. Numerical Heat Transfer and Fluid Flow. Hemisphere Publishing Corporation, 1980.

[6] Rhie, C.M. and Chow, W.L. Numerical study of the turbulent flow past an airfoil with training edge separation. *AIAA Journal*, **21**, (1983), 1525–1532.

[7] Wathen, A.J., Ẽlman, H.C. and Silvester, D. Finite Elements and Fast Iterative Solvers, Oxford University Press, Oxford, 2005

Appendix

A Bessel functions

Bessel functions are necessary to solve the system (11) to (14) in Section 4. These functions are defined as follows:

$$
\begin{aligned}
I_0(x) &= \sum_{k=0}^{\infty} \frac{x^{2k}}{4^k (k!)^2} \ , \\
I_1(x) &= I_0'(x) = \sum_{k=1}^{\infty} \frac{(2k) x^{2k-1}}{4^k (k!)^2} \ , \\
K_0(x) &= -I_0(x) \left[\ln\left(\frac{x}{2}\right) + \gamma \right] + \sum_{k=1}^{\infty} \frac{x^{2k} \psi(k)}{4^k (k!)^2} \ , \\
K_1(x) &= -K_0'(x) = I_1(x) \left[\ln\left(\frac{x}{2}\right) + \gamma \right] + \frac{I_0(x)}{x} - \sum_{k=1}^{\infty} \frac{(2k) x^{2k-1} \psi(k)}{4^k (k!)^2} \ ,
\end{aligned}
$$

where $\gamma = 0.57721566$ is the Euler constant and

$$
\psi(k) = \sum_{i=1}^{k} \frac{1}{k} \ .
$$

In the present code, the functions were approximated using sums up to $k_{max} = 30$, this is high enough to calculate accurate values. Many other choices are possible.

B Analytical solution for the system in Section 4.2

An analytical solution for the system (11) to (14) may be calculated using the continuity of temperatures and heat fluxes:

$$0 \le r \le r_1 : \qquad T = \alpha I_0\left(r_1\sqrt{\frac{H}{\kappa_2}}\right) + \beta K_0\left(r_1\sqrt{\frac{H}{\kappa_2}}\right) + \frac{q + HT_g}{H}\ , \quad (25)$$

$$r_1 \le r \le r_2 : \qquad T = \alpha I_0\left(r\sqrt{\frac{H}{\kappa_2}}\right) + \beta K_0\left(r\sqrt{\frac{H}{\kappa_2}}\right) + \frac{q + HT_g}{H}\ , \quad (26)$$

$$r_2 \le r \le r_3 : \qquad T = T_0 + \gamma \ln\left(\frac{r}{r_3}\right)\ , \quad (27)$$

where I_0 and K_0 are the modified Bessel functions (see Appendix A). The constants are defined by:

$$\alpha = \frac{\kappa_3\gamma}{r_2\sqrt{H\kappa_2}} \times \frac{K_1\left(r_1\sqrt{(H/\kappa_2)}\right)}{I_1\left(r_2\sqrt{(H/\kappa_2)}\right)K_1\left(r_1\sqrt{(H/\kappa_2)}\right) - I_1\left(r_1\sqrt{(H/\kappa_2)}\right)K_1\left(r_2\sqrt{(H/\kappa_2)}\right)}\ ,$$

$$\beta = \frac{\kappa_3\gamma}{r_2\sqrt{H\kappa_2}} \times \frac{I_1\left(r_1\sqrt{(H/\kappa_2)}\right)}{I_1\left(r_2\sqrt{(H/\kappa_2)}\right)K_1\left(r_1\sqrt{(H/\kappa_2)}\right) - I_1\left(r_1\sqrt{(H/\kappa_2)}\right)K_1\left(r_2\sqrt{(H/\kappa_2)}\right)}\ ,$$

$$\gamma = \left(\frac{q + HT_g}{H} - T_0\right) \Big/ \left(\ln\left(\frac{r_2}{r_3}\right) - \Delta\right)\ ,$$

$$\Delta = \frac{\kappa_3}{r_2\sqrt{H\kappa_2}} \times \frac{I_1\left(r_1\sqrt{(H/\kappa_2)}\right)K_0\left(r_2\sqrt{(H/\kappa_2)}\right) + I_0\left(r_2\sqrt{(H/\kappa_2)}\right)K_1\left(r_1\sqrt{(H/\kappa_2)}\right)}{I_1\left(r_2\sqrt{(H/\kappa_2)}\right)K_1\left(r_1\sqrt{(H/\kappa_2)}\right) - I_1\left(r_1\sqrt{(H/\kappa_2)}\right)K_1\left(r_2\sqrt{(H/\kappa_2)}\right)}$$

and the functions I_1 and K_1 are modified Bessel functions defined in Appendix A.